

Article

Metallosupramolecular Compounds Based on Copper(II/I) Chloride and Two Bis-Tetrazole Organosulfur Ligands

Olaya Gómez-Paz ¹, Rosa Carballo ^{1,*}, Ana Belén Lago ^{2,*} and Ezequiel M. Vázquez-López ¹

¹ Departamento de Química Inorgánica, Instituto de Investigación Sanitaria Galicia Sur (IISGS)-Universidade de Vigo, 36310 Vigo, Galicia, Spain; olgomez@uvigo.es (O.G.-P.); ezequiel@uvigo.es (E.M.V.-L.)

² Departamento de Química, Facultad de Ciencias, Sección Química Inorgánica, Universidad de la Laguna, 38206 La Laguna, Spain

* Correspondence: rcrial@uvigo.es (R.C.); alagobla@ull.edu.es (A.B.L.)

Received: 13 January 2020; Accepted: 29 January 2020; Published: 4 February 2020



Abstract: The present work assesses the ability of two flexible bis-tetrazole organosulfur ligands to build up different metallosupramolecular compounds based on the analysis of the different supramolecular interactions. The reaction of copper(II) chloride dihydrate with the *N,N'*-donor dithioether ligands bis(1-methyl-1*H*-tetrazole-5-ylthio)methane (BMTTM) and 1,2-bis(1-methyl-1*H*-tetrazole-5-ylthio)ethane (BMTTE) was investigated using different synthetic methods. Four compounds have been obtained as single crystals: two pseudopolymorphic 1D Cu(II) coordination polymers with the ligand BMTTM, a 2D Cu(II) coordination polymer and a discrete Cu(I) tetramer with the BMTTE ligand. The effects of the weak interactions on the crystal packing and the Hirshfeld surfaces of the structures were analyzed to clarify the nature of the intermolecular interactions.

Keywords: copper chloride complexes; H-bonding pattern; tetrazole ligands; X-ray diffraction; Hirshfeld surfaces

1. Introduction

Structurally well-defined supramolecular architectures produced by the formation of ordered crystalline materials have attracted considerable attention in recent years due to their different novel chemical properties and their possible new applications. Coordination chemistry has played a central role in the blossoming of this fast-evolving field. In this way, metallosupramolecular chemistry, which concerns non-covalent interactions between discrete or polymeric coordination compounds, has become an interdisciplinary research area that has provided insights into and spurred developments across biology, chemistry, nanotechnology, materials science and physics [1].

Amongst the metallosupramolecular compounds, supramolecular metal–organic frameworks (SMOFs) are materials that can be considered as analogs to metal–organic frameworks (MOFs) in the sense that some coordination bonds are replaced by hydrogen bonds as directional interactions to build the final crystal. In SMOFs, the coordination bonds are released from guiding the crystal structure and supramolecular interactions play this role instead. The strategy for the preparation of SMOFs is based on the synthesis of coordination compounds, with the choice of metal center made on the basis of its coordinative preferences and the ligand or a combination of ligands with the ability to coordinate the metal cation and also facilitate several weak interactions between the diverse rigid molecular units [2].

The final goal of supramolecular chemistry is to understand the inherent complexities of the association mechanisms of molecular and ionic building blocks organized through multiple noncovalent

interactions [3,4]. The relatively greater strength of ligand–metal coordination bonds when compared with other noncovalent interactions allows the stabilization of a range of different structures, whereas the weak and reversible forces are key to understanding these self-assembling systems. In terms of the weak intermolecular noncovalent interactions, the analysis of C–H···X (X = Cl, S, N) hydrogen bonds in metallosupramolecular systems has received less attention despite its proven participation in several biological systems [5,6]. In this way, the hydrogen bond acceptor capability of halogens has attracted attention on a number of fronts. In the context of metallosupramolecular chemistry, halide ligands (M–X) have been used to drive the self-assembly of coordination compounds due to their directionality and versatility [7,8].

In order to facilitate the hydrogen bond acceptor role of a halide, such as chloride in a SMOF, copper(II) chloride is used as the metal source and, although the Cu(II) cation is stable under ambient conditions, Cu(II)-to-Cu(I) transformations at room temperature can be produced by reaction conditions such as temperature, pH value, solvents and pressure due to the low standard electrode potential between Cu(II) and Cu(I).

The tetrazole organosulfur derivatives and their transition metal complexes are important in medicinal chemistry and drug design [9] and also as industrial materials [10]. In the field of metallosupramolecular chemistry, these compounds are particularly interesting since the tetrazole moiety contains several nitrogen atoms that can facilitate simultaneously the coordination to one or more metal centers and the formation of hydrogen bonds acting as acceptors.

With the aim of studying the role of C–H···X (X = Cl, S, N) hydrogen bonds in the crystalline supramolecular networks based on copper(II/I) chloride/bis-tetrazole organosulfur systems, we report here the crystal structures of four compounds resulting from reactions under different synthetic conditions between the ligands bis(1-methyl-1H-tetrazole-5-ylthio)methane (BMTTM) and 1,2-bis(1-methyl-1H-tetrazole-5-ylthio)ethane (BMTTE) and copper(II) chloride. These ligands have attractive features, such as the multiple heteroatomic potential coordination sites, six N donors and two S atoms, which also contribute to the flexibility of the ligands. In both ligands, there are three adjacent N donors in each methyl-tetrazole group, and these may promote the construction of multinuclear clusters.

In the literature there is structural information on several compounds based on copper(II/I) polyoxometalates (POMs = $\text{H}_2\text{Mo}_8\text{O}_{26}^{2-}$, $\text{PMo}_{12}\text{O}_{40}^{3-}$, $\text{SiW}_{12}\text{O}_{40}^{3-}$, $\text{PW}_{12}\text{O}_{40}^{3-}$, $\text{SiMo}_{12}\text{O}_{40}^{4-}$, $\text{SiW}_{12}\text{O}_{40}^{4-}$, $\text{HSiMo}_{12}\text{O}_{40}^{3-}$) and these two ligands [11–14]. These compounds are 1D, 2D or 3D coordination polymers in which the ligands are able to coordinate two, three or four copper cations by chelating and/or bridging coordination modes. However, a study of the weak interactions responsible for the supramolecular organization has not been undertaken for any of these compounds.

2. Results and Discussion

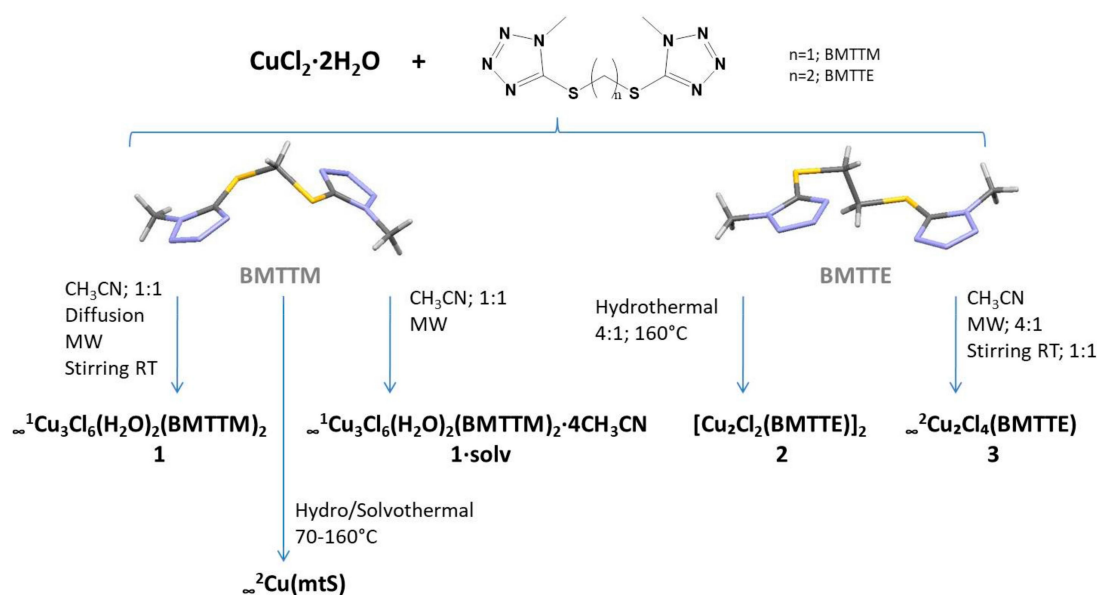
2.1. Synthesis of the Complexes

The study of the reactivity in the $\text{CuCl}_2/\text{BMTTM}$ or BMTTE system was performed using different stoichiometric ratios and four synthetic methods: stirring at room temperature, diffusion, reflux under microwave irradiation and hydro/solvothermal techniques. Conventional synthesis at room temperature afforded the compounds in good yields. However, hydrothermal and microwave methods, providing the same compounds in lower yields, were used to synthesize compounds as pure materials and as single crystals. Acetonitrile was used as the solvent for the reactions due to the better solubility of the ligands in this solvent. The synthetic conditions allowed the preparation of the crystalline complexes **1**, **1-solv**, **2** and **3** (Scheme 1).

In the reactions of copper(II) chloride with BMTTM, compound **1** was obtained in good yield with a 1:1 metal/ligand ratio by diffusion and by stirring at room temperature. However, when the reaction was performed under microwave irradiation, in addition to **1**, some crystals of the pseudopolymorph **1-solv** (4CH₃CN) were also obtained. The hydro/solvothermal methods tested at different metal/BMTTM

ligand ratios at different temperatures between 70 and 160 °C in all cases yielded the copper(I) 2D coordination polymer **Cu(mtS)** (mtS = 1-methyl-1*H*-tetrazole-5-thiolato) [15], which indicates that cleavage of the BMTTM ligand had taken place under these synthetic conditions.

Reactions with BMTTE were conditioned by its low solubility in all of the solvents tested and, as a consequence, a copper complex could not be isolated by diffusion due to the rapid crystallization of BMTTE [16,17]. Copper(II) compound **3** was obtained as an orange crystalline powder upon stirring at room temperature using a 1:1 molar ratio, and as orange single crystals by reaction under microwave irradiation using a 4:1 metal/ligand molar ratio. The copper(I) complex **2** was obtained under hydrothermal conditions at 160 °C with a 3:1 metal/ligand ratio. This hydrothermal reduction of copper(II) to copper(I) was previously observed in the preparation of copper polyoxometalates of BMTTM and BMTTE from copper(II) acetate, although the authors indicated that metal/ligand ratios greater than 10:1 are required for this reduction to occur [11–14].



Scheme 1. Summary of the synthetic routes for the complexes and the Cu(II):L stoichiometric ratios, temperature and solvent used where relevant (RT: room temperature; MW: microwave).

2.2. Structural Studies: General Features

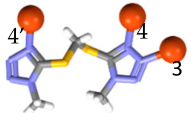
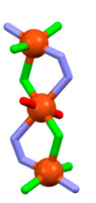
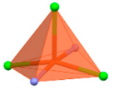
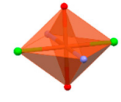
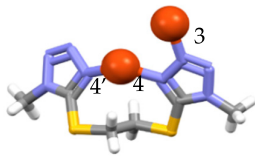
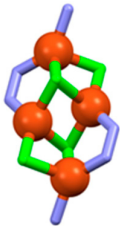

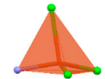
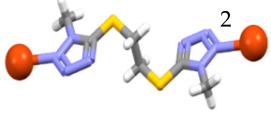
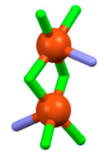
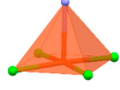
All of the compounds described here were isolated as single crystals and their structures were elucidated by X-ray diffraction. The combination of the flexible polydentate ligands with different chlorocuprate clusters resulted in the formation of 1D coordination polymer chains (**1** and **1-solv**) or a 2D coordination layer (**3**). Moreover, the reduction of copper(II) to copper(I) produced a stable discrete tetrameric Cu(I) coordination compound (**2**). The main structural features for each compound are provided in Table 1. The structures can be deconstructed into two components: trinuclear units $\{\text{Cu}_3\text{Cl}_6\text{N}_6\text{O}_2\}$ in **1** and **1-solv**, tetranuclear units $\{\text{Cu}_4\text{Cl}_4\text{N}_6\}$ in **2**, and dinuclear units $\{\text{Cu}_2\text{Cl}_4\text{N}\}$ in **3** as inorganic chlorocuprate building clusters, and the corresponding flexible BMTTM and BMTTE tetrazole bridging ligands.

The two methyl tetrazole groups in BMTTM and BMTTE are separated by a flexible organosulfur spacer that allows rotation around the C–S and C–C bonds to adjust the direction of the coordination nitrogen atoms. It is therefore apparent that the rigid and geometrically well-defined structures of the inorganic units with the flexibility and the potential N-hexacoordination ligands are essential to achieve the structural diversity observed in these systems.

Compounds **1**, **1-solv** and **3** are polymeric coordination compounds. The layers of **3** are formed by chloride-bridged $\text{Cu}(\mu\text{-Cl})_2$ chains and bridging N-donor ligands in a second dimension that act as cross-linking ligands. The copper-chloride chain is based on the repetition of the dinuclear Cu_2Cl_2

unit, as shown in Table 1. The polymeric chains of **1** and **1·solv** incorporate trinuclear Cu_3Cl_6 units and organic subunits in an alternate manner.

Table 1. Main structural features.

Compound Dimensionality	Coordination Mode of Ligand	Inorganic Units	Coordination Geometry
$\infty^1\text{Cu}_3\text{Cl}_6(\text{H}_2\text{O})_2(\text{BMTTM})_2$ (1) 1D			 Cu2
$\infty^1\text{Cu}_3\text{Cl}_6(\text{H}_2\text{O})_2(\text{BMTTM})_2 \cdot 4\text{CH}_3\text{CN}$ (1·solv) 1D	$\mu_3\text{-}1\kappa\text{N}3:2\kappa\text{N}4:3\kappa\text{N}4'$	$\{\text{Cu}_3\text{Cl}_6\text{N}_6\text{O}_2\}$	 Cu1
$[\text{Cu}_2\text{Cl}_2(\text{BMTTE})]_2$ (2) 0D, tetramer			 Cu1
	$\mu\text{-}1\kappa^2\text{N}4, \text{N}4':2\kappa\text{N}3$	$\{\text{Cu}_4\text{Cl}_4\text{N}_6\}$	 Cu2
$\infty^2\text{Cu}_2\text{Cl}_4(\text{BMTTE})$ (3) 2D			 Cu2
	$\mu\text{-}\kappa\text{N}2$	$\{\text{Cu}_2\text{Cl}_4\text{N}\}$	

Compound **2** is a discrete tetrameric compound based on a stair-step Cu_4Cl_4 cluster coordinated by two BMTTE ligands in an octahedral $\{\text{Cu}_4\text{Cl}_4\text{N}_6\}$ motif, which has been less widely studied than other copper halide clusters such as cubane organizations. In this octahedral motif, a tetranuclear copper core defines the basal plane of an octahedron with two capping μ_3 -chloride atoms in the apical positions and bridging μ_2 -chloride and nitrogen BMTTE atoms along the meridian positions [18].

2.3. Crystal Structures of **1** and **1·solv**

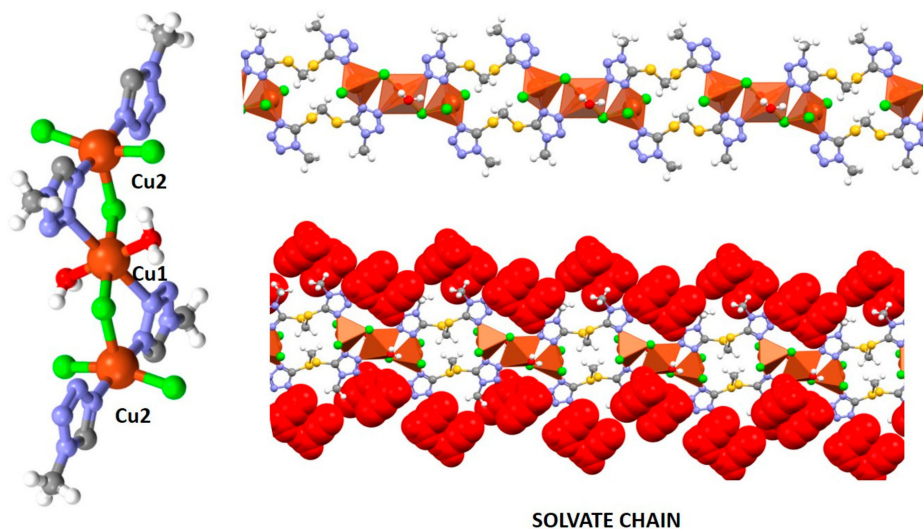
Complex **1** and the solvate **1·solv** crystallize in the monoclinic $P2_1/n$ and triclinic $P-1$ space groups, respectively, and they could be considered pseudopolymorphs [19] since they have the same crystalline form, although **1·solv** crystallizes with acetonitrile molecules trapped within the crystal network. Significant structural parameters for compounds **1–1·solv** are listed in Table 2 and crystal structure and refinement data are listed in Table S1. Both structures are 1D chains based on a $\{\text{Cu}_3\text{Cl}_6\}$ cluster and the BMTTM ligand, as shown in Figure 1. The three copper atoms in the $\{\text{Cu}_3\text{Cl}_6\}$ unit are aligned with a $\text{Cu}1\text{--Cu}2\text{--Cu}1$ angle of 180° [20]. The conformation of the outer two coppers is identical. The $\text{Cu}1 \cdots \text{Cu}2$ distance is 3.903 Å in **1** and slightly shorter (3.842 Å) in **1·solv**.

Table 2. Selected bond lengths/Å and angles/°.

Atoms	1	1·solv	Atoms	1	1·solv
Cu1–Cl1	2.5477(12)	2.5119(4)	N4–Cu1–N8#1	171.83(15)	174.19(4)
Cu1–Cl2	2.2895(11)	2.2660(4)	N8#1–Cu1–Cl1	93.88(11)	93.94(3)
Cu1–Cl3	2.2744(12)	2.2927(3)	N8#1–Cu1–Cl2	90.83(11)	90.23(3)
Cu2–N3	2.561(4)	2.4137(11)	N8#1–Cu1–Cl3	90.22(11)	87.76(3)
Cu1–N4	2.038(4)	2.0500(11)	Cl1#2–Cu2–Cl1	180.00(5)	180.000(14)
Cu1–N8#1	2.052(4)	2.0346(11)	Cl1–Cu2–N3	83.54(9)	85.98(3)
Cu2–Cl1	2.2981(10)	2.2716(3)	Cl1–Cu2–N3#2	96.46(9)	94.02(3)
Cu2–Cl1#2	2.2980(10)	2.2716(3)	N3#2–Cu2–N3	180.0	180.0
Cu2–O1	1.959(3)	2.0140(9)	O1–Cu2–Cl1	90.18(10)	88.06(3)
Cl2–Cu1–Cl1	97.16(4)	102.660(12)	O1–Cu2–Cl1#2	89.82(10)	91.94(3)
Cl3–Cu1–Cl1	105.98(4)	100.253(12)	O1–Cu2–N3	89.96(14)	93.80(4)
Cl3–Cu1–Cl2	156.72(4)	157.082(13)	O1#2–Cu2–N3	90.03(13)	86.20(4)
N4–Cu1–Cl1	94.23(11)	91.57(3)	O1–Cu2–O1#2	180.0	180.00(5)
N4–Cu1–Cl2	87.23(11)	90.35(3)	Cu2–Cl1–Cu1	107.19(4)	106.772(12)
N4–Cu1–Cl3	88.45(11)	89.45(3)			

Symmetry code: (1) #1 $-x + 2, -y + 1, -z + 1$; #2 $-x + 1, -y + 2, -z + 1$; (1·solv) #1 $-x + 1, -y + 1, -z + 2$; #2 $-x + 1, -y + 2, -z + 2$.

The two bridges of chloride and N–N tetrazole atoms between the Cu1 and Cu2 lead to the formation of an unusual planar $\{\text{Cu}_3\text{Cl}_6\text{N}_6\text{O}_2\}$ cluster. These units are connected by two BMTTM ligands to form infinite tapes, as shown in Figure 1.

**Figure 1.** Coordination environments and polymeric chains of **1** and **1·solv**.

The Cu1 center is pentacoordinated and the value of the Addison parameter [21] τ of 0.25 (0.28 in **1·solv**) indicates a square pyramidal coordination geometry around this copper atom, with the two nitrogen atoms and the two terminal chloride atoms in the *trans* positions of the pyramid base and a chloride atom acting as a bridge between Cu1 and Cu2 at the apex position. The Cu–Cl bond lengths with the chloride terminal groups are in the range 2.27–2.29 Å and the bridging chloride atom in the apical position is located at a longer distance, with Cu–Cl distances of 2.5477(12) Å in **1** and 2.5119(4) Å in **1·solv**.

The Cu2 atom is in an elongated octahedral environment and it exhibits the expected Jahn–Teller distortion, with four short metal–ligand bonds (Cu–Ow and Cu–Cl) and two long bonds with nitrogen atoms of BMTTM bridging ligands [Cu2–N distances of 2.561(4) and 2.4137(11) Å in **1** and **1·solv**, respectively]. Here, it is worth highlighting the equatorial coordination position of the water molecule, which contrasts with the typical axial position in similar systems.

The BMTTM ligand uses three nitrogen atoms of the two tetrazole rings to coordinate three metal centers, as shown in Table 2, with a bridging role that results in the formation of a tape, as shown in Figure 1, with 16-membered macrocycles ($\text{Cu}_2\text{N}_4\text{S}_4\text{C}_6$). This macrocyclic motif has previously been observed in complexes with other thioether N-donor ligands [22]. This coordination mode ($\mu_3\text{-}1\kappa\text{N}3\text{:}2\kappa\text{N}4\text{:}3\kappa\text{N}4'$) of BMTTM was not observed in the copper-POM complexes, in which the ligand had a bidentate chelating coordination mode with one, two or three copper cations [12,14]. The intermetallic distances through the BMTTM-bridge are 6.97 Å for compound **1** and 6.69 Å for **1·solv**. Moreover, the intramolecular N···N distance is shorter in **1·solv** (6.48 Å) than in **1** (6.70 Å). On comparing the two structures, it is evident that BMTTM acts as a semirigid ligand, which shrinks due to the presence of the guest molecules in **1·solv** but retains the same connectivity and geometric environment in both cases. In accordance with this situation, the value of the C–S–C–S torsion angles are 81.78° and 83.20° in **1** and 77.14° and 84.45° in **1·solv**. The chains are achiral and incorporate molecules of BMTTM with opposite helicity in each macrocycle unit.

2.4. Crystal Structure of **2**

The Cu(I) compound **2** crystallizes in the $P2_1/n$ space group with an inversion center located between the Cu2 central atoms. Significant structural parameters are listed in Table 3, and crystal structure and refinement data are listed in Table S1. Four Cu(I) atoms and four chloride atoms form a stair-like $[\text{Cu}_4\text{Cl}_4]$ cluster core with each of the two BMTTE ligands anchored at each end of the stair through two Cu(I) centers, as shown in Figure 2 [23,24]. In the cluster, the $\text{Cu}2\cdots\text{Cu}2$ distance of 2.7651(5) Å is slightly shorter than the sum of the van der Waals radii of two Cu atoms (2.80 Å), thus indicating attractive $\text{Cu}\cdots\text{Cu}$ interactions, but the $\text{Cu}1\cdots\text{Cu}2$ distance of 2.9556(3) Å suggests that copper–copper interactions are not present [25].

Table 3. Selected bond lengths/Å and angles/°.

Atoms	2	3	Atoms	2
Cu1–Cu2#1	2.9556(3)		N4–Cu1–Cu2#1	124.81(4)
Cu1–Cl1	2.4039(4)	2.3132(4)	N4–Cu1–Cl1	106.22(4)
Cu1–Cl1#2		2.3163(4)	N4–Cu1–Cl2#1	96.70(4)
Cu1–Cl2		2.2987(4)	N4–Cu1–N8	137.74(6)
Cu1–Cl2#1	2.4794(4)	2.2979(4)	N8–Cu1–Cu2#1	96.92(4)
Cu1–N2		2.3981(13)	N8–Cu1–Cl1	100.74(4)
Cu1–N4	2.0097(14)		N8–Cu1–Cl2#1	108.89(4)
Cu1–N8	2.0268(14)		Cu2#1–Cu2–Cu1#1	72.140(10)
Cu2–Cu2#1	2.7651(5)		Cl1–Cu2–Cu1#1	111.431(14)
Cu2–Cl1	2.3556(5)		Cl1–Cu2–Cl1#1	113.629(13)
Cu2–Cl1#1	2.6728(5)		Cl1#1–Cu2–Cl1#1	50.261(10)
Cu2–Cl2	2.2330(4)		Cl1#1–Cu2–Cu2#1	51.302(12)
Cu2–N7	2.0013(14)		Cl1–Cu2–Cu2#1	62.326(13)
Cl1–Cu1–Cu2#1	58.759(12)		Cl2–Cu2–Cu1#1	54.982(12)
Cl2#1–Cu1–Cu2#1	47.525(11)		Cl2–Cu2–Cu2#1	121.487(16)
Cl1–Cu1–Cl1#2		176.292(10)	Cl2–Cu2–Cl1	113.376(17)
Cl2–Cu1–Cl1		93.746(16)	Cl2–Cu2–Cl1#1	100.991(16)
Cl2#1–Cu1–Cl1	102.006(16)	85.599(15)	N7–Cu2–Cu1#1	137.43(4)
Cl2#1–Cu1–Cl1#2		94.895(15)	N7–Cu2–Cu2#1	99.24(4)
Cl2–Cu1–Cl1#2		85.511(15)	N7–Cu2–Cl2	135.88(4)
Cl2#1–Cu1–Cl2		176.067(11)	N7–Cu2–Cl1	99.50(4)
Cl1–Cu1–N2		96.33(3)	N7–Cu2–Cl1#1	91.18(4)
Cl1#2–Cu1–N2		87.29(3)	Cu2–Cl2–Cu1#1	77.492(15)
Cl2–Cu1–N2		88.39(3)	Cu1–Cl1–Cu2#1	70.981(13)
Cl2#1–Cu1–N2		95.53(3)	Cu2–Cl1–Cu1	90.204(15)
Cu1#2–Cu1–N2		90.896(14)	Cu2–Cl1–Cu2#1	66.371(14)
Cu1–Cl1–Cu1#1		90.072(14)		

Symmetry code: (2) #1 $-x + 1, -y + 2, -z + 1$; (3) #1 $-x + 1/2, y + 1/2, -z + 3/2$; #2 $-x + 1/2, y - 1/2, -z + 3/2$.

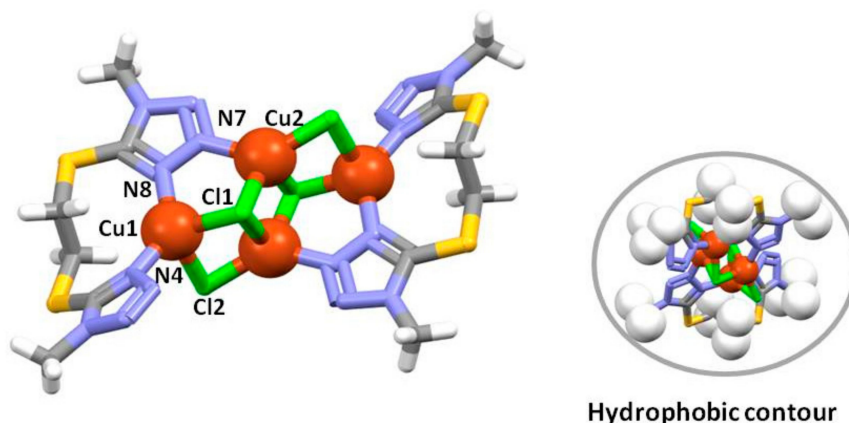


Figure 2. Molecular structure of **2** showing the hydrophobic contour of the tetrameric unit.

The chloride ligands display μ_3 -Cl1 and μ -Cl2 bridging modes. Each Cu(I) center is tetrahedrally coordinated—Cu1 by two BMTTE nitrogen atoms and Cl1 and Cl2 atoms, and Cu2 by one BMTTE nitrogen atom, two μ_3 -Cl1 and one μ -Cl2 atoms, so the values of the τ_4 parameters [26] of 0.80 for Cu1 and 0.77 for Cu2 indicate a fairly regular tetrahedral geometry. Cl2, which is bonded to adjacent copper atoms with Cu–Cl distances of 2.4794(4) Å and 2.2330(4) Å, resides 0.813 Å above and below the planar copper core. The triply bonded chloride ligand connects Cu1 and Cu2 atoms with variable distances [2.4039(4) Å, 2.3556(5) Å and 2.6728(5) Å].

In compound **2**, each BMTTE molecule provides three N atoms to coordinate two copper ions, as shown in Figure 2. Thus, BMTTE acts as a bis-monodentate bridging ligand to link Cu1 and Cu2 through the tetrazole fragment and also as a bidentate chelating ligand with Cu1 to give a nine-membered ring ($\text{CuN}_2\text{S}_2\text{C}_4$). This coordination mode of BMTTE has also been observed in a copper-POM 1D coordination polymer [13]. The S–C–C–S torsion angle is 168.93° and the two ligands in the tetramer have opposite axial chirality.

2.5. Crystal Structure of **3**

The Cu(II) polymeric compound **3** crystallizes in the $C2/c$ space group with one crystallographically independent copper atom. Significant structural parameters are listed in Table 3, and crystal structure and refinement data are listed in Table S1. A dimeric Cu_2Cl_4 motif with two metal cations linked by two bridging chloride atoms leads to the formation of Cu_2Cl_4 -based inorganic chains along the b axis, as shown in Figure 3. The nonbonding $\text{Cu}\cdots\text{Cu}$ distance through the halide bridge is 3.276 Å. These chains are bridged by bis-monodentate BMTTE ligands to yield the final 2D coordination compound. The 2D structure contains 32-membered macrometalloclusters formed by (Cu_3Cl_4) inorganic units and two BMTTE ligands, as shown in Figure 3, with the methyl groups of each ligand molecule orientated to opposite sides.

The copper(II) cation is pentacoordinated, as shown in Figure 3, and the value of the Addison parameter τ [21] of 0.04 indicates that the coordination sphere is almost an ideal square pyramid, with four chloride atoms in basal positions (Cu–Cl distances between 2.313 and 2.298 Å) and a nitrogen atom belonging to a BMTTE molecule at the apex (Cu–N2 = 2.3981(13) Å). At a longer distance (2.854 Å) in the sixth coordination position is a nitrogen atom (N3) of an opposite ligand molecule, so that each tetrazole group coordinates a metal center and establishes a weak contact with a neighboring metal center.

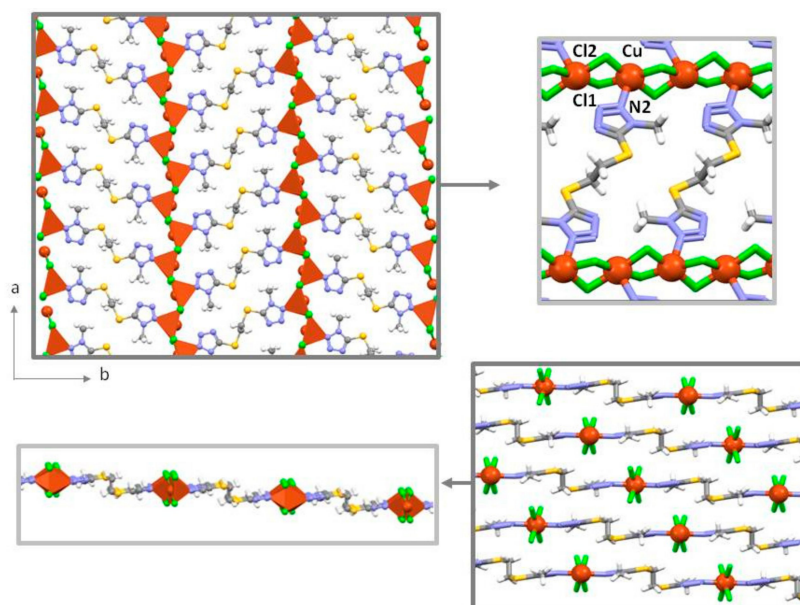


Figure 3. Top; 2D structure of **3** showing in detail the macrometallocycle. Bottom; supramolecular arrangement of the layers.

The BMTTE acts as a bis-monodentate bridging (μ - κ N2) ligand. This coordination mode is different to the bis-monodentate bridging mode observed in some copper-POM complexes, where the nitrogen atom involved in coordination is N3 [11,12] and not N2. The S–C–C–S torsion angle is 180° and each metallocycle contains two ligands of opposite chirality to yield an achiral layer. The distance between two neighboring copper(II) ions through the BMTTE ligand is 14.585 \AA and the intramolecular N \cdots N distance is 9.794 \AA .

2.6. Supramolecular Arrangements

The strategic use of supramolecular synthons to control crystal structure allows the design of new solids with interesting physicochemical properties. However, to achieve this objective, it is necessary to understand the intermolecular interactions in the context of crystal packing. In the current systems, common structural and compositional characteristics allow a deeper study of this aspect. In this sense, chloride ligands have shown through crystallographic data analysis that the weak C–H \cdots Cl–M interactions exhibit the characteristics of conventional hydrogen bonds and hence are very significant in molecular recognition and crystal engineering. Another interesting feature in these structures is the presence of coordinatively unsaturated metal centers (UMCs), which can interact at longer distances with other atoms. Besides, it should be noted in these compounds that not all of the nitrogen atoms of each tetrazole take part in coordination, so free N-atoms are still available to act as hydrogen acceptors in different interactions, thus playing a significant role in the final supramolecular arrangements. Moreover, the flexible organosulfur chains between the tetrazole groups offer the possibility of establishing noncovalent interactions involving the sulfur atom as an acceptor or the organic fragment as a donor. In addition, the methyl substituent in the tetrazole moiety increases the hydrophobicity and the stability of the molecules, but the most remarkable feature observed in these structures is its role as a donor in multiple interactions.

In this way, chains of **1** are organized into a supramolecular 2D network along the *ab* plane by means of O–H \cdots Cl hydrogen bonds that involve coordinated water molecules and chloride atoms of neighboring chains. Nonpolar hydrophobic methyl groups are oriented out of the layers and establish C–H \cdots Cl interactions with other chains to give the final 3D supramolecular array, as shown in Figure 4. An interchain Cl \cdots π interaction [Cl2 \cdots centroid of N1/N2/N3/N4/C1; $d(\text{Cl}\cdots\text{centroid}) = 3.355 \text{ \AA}$; $1 - x$,

$2 - y, 1 - z$] and $\text{CH}_{\text{Me}} \cdots \text{N}$ and $\text{CH}_{\text{Me}} \cdots \text{S}$ interactions, as shown in Table 4, also participate in the formation of the crystal network, which has a Kitaigorodskii packing index [27] of 75%.

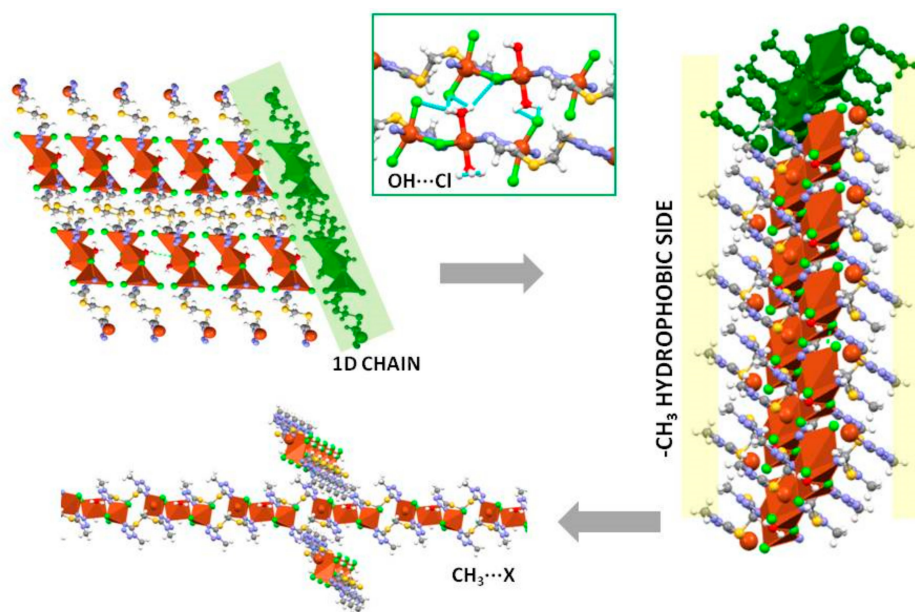


Figure 4. Supramolecular arrangement in the crystal structure of **1**.

The supramolecular arrangement in **1-solv** is mainly due to $\text{C-H} \cdots \text{X}$ interactions ($\text{X} = \text{Cl}$ and N) but, as observed in similar compounds [28], solvent molecules are involved in different $\text{C-H} \cdots \text{X}$ ($\text{X} = \text{Cl}, \text{O}, \text{N}$; Table 4) interactions with the metal–organic framework, so the polymeric chains are extended along the b axis and arranged in a sinusoidal manner, with solvent molecules hosted between them, as shown in Figure 5. These hydrogen-bonding interactions are established between the methyl groups of tetrazole or acetonitrile as donors with the available nitrogen atoms of both fragments as acceptors. The metallorganic chains are linked through solvent molecules that act as a bridge in the ac plane, as shown in Figure 5 (top, left), to give a shifted parallel arrangement. Furthermore, several weak intra- and inter-molecular $\text{C-H} \cdots \text{S}$ interactions reinforce the zig-zag disposition of the chains. The solvent volume makes up 30% of the unit cell volume, as calculated using Mercury [29], and the Kitaigorodskii packing index [27] of 75% is slightly lower than that in **1**.

In the crystal packing of **2**, the nonpolar methyl $-\text{CH}_3$ and methylene $-\text{CH}_2-$ spacer groups, which are oriented outwards from the tetrameric molecule to define a hydrophobic contour, as shown in Figure 2, play an important role as H-donors towards the chloride atoms to establish several intermolecular $\text{C-H} \cdots \text{Cl}$ interactions with $\text{C} \cdots \text{Cl}$ distances in the range 3.32–3.47 Å, as shown in Table 4 and Figure 6. This kind of interaction is also established with the nitrogen atoms of tetrazole units. Furthermore, a $\pi \cdots \pi$ interaction between the tetrazole groups N1/N2/N3/N4/C1 and N5/N6/N7/N8/C4 (intermolecular centroid–centroid distance of 3.6976 Å and interplanar dihedral angle of 33.40°; symmetry code: $1 - x, 1 - y, 1 - z$) contributes to the crystal packing, with a Kitaigorodskii index [27] of 70%.

The metallorganic layer of **3** has a stair-step disposition along the ab plane, as shown in Figure 3, and each layer stacks with adjacent ones through $\text{CH}_{\text{methylene}} \cdots \text{Cl}$ interactions, as shown in Table 4, to give a 3D supramolecular array reinforced by the contribution of an $\text{S} \cdots \pi$ interaction with the tetrazole ring ($\text{S} \cdots$ centroid distance = 3.357 Å; symmetry: $1 - x, y, 1.5 - z$). The resulting Kitaigorodskii packing index [27] is 77%.

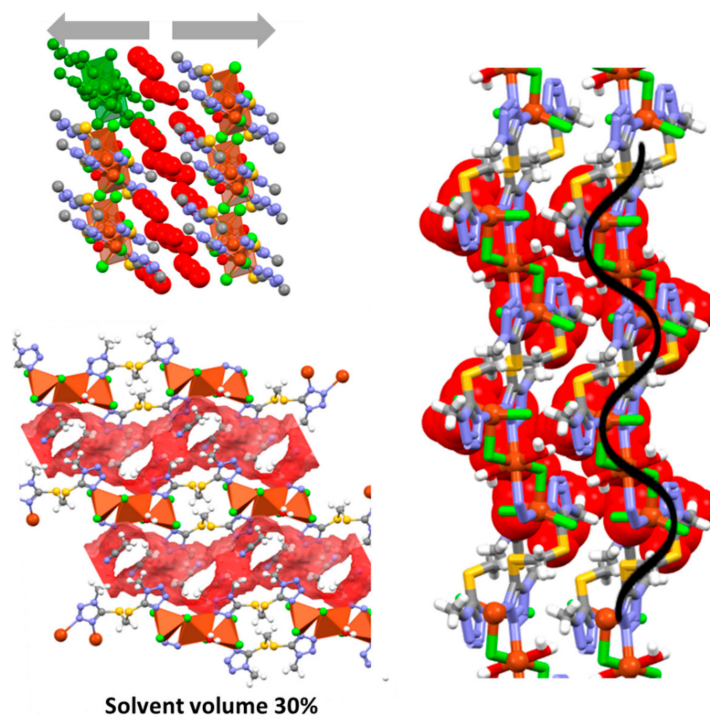


Figure 5. Supramolecular arrangement in the crystal structure of **1·solv**.

Table 4. Main hydrogen bonds (Å, °).

Structure	D–H···A	d(D–H)	d(H···A)	d(D···A)	∠(DHA)
1	O1–HA ... Cl3#1	0.84(2)	2.82(6)	3.250(4)	114(5)
	O1–HA ... Cl1#1	0.84(2)	2.93(4)	3.685(3)	152(6)
	C12–H12C ... Cl2#4	0.98	2.49	3.418(5)	158.6
	C12–H12B ... N7#3	0.98	2.86	3.207(6)	102.0
	C12–H12A ... N6#2	0.98	2.68	3.327(6)	124.0
	C12–H12A ... S2#1	0.98	2.90	3.717(5)	141.2
1·solv	O1–H1C ... Cl1#6	0.89	2.99	3.6713(10)	135.4
	O1–H1C ... Cl2#6	0.89	2.72	3.4096(10)	135.1
	C12–H12C ... N41#7	0.98	2.95	3.221(2)	96.9
	C12–H12B ... N31#4	0.98	2.68	3.650(2)	170.0
	C22–H22C ... Cl3#5	0.98	2.95	3.5901(15)	123.9
	C1–H1B ... Cl2#3	0.99	2.95	3.5478(13)	119.9
	C1–H1B ... S2#2	0.99	2.95	3.5065(13)	116.3
	C31–H31A ... N6#5	0.98	2.64	3.559(2)	156.5
	C31–H31B ... N7#1	0.98	2.59	3.473(2)	150.1
	C31–H31C ... O1#7	0.98	2.71	3.536(2)	141.7
C41–H12A ... Cl1#6	0.98	2.98	3.3693(15)	104.8	
2	C2–H2B ... Cl2#1	0.99	2.89	3.3201(17)	107.2
	C1–H1B ... Cl2#1	0.99	2.84	3.4698(17)	122.1
	C12–H12C ... Cl2#3	0.98	2.87	3.4037(19)	115.0
	C22–H22C ... Cl1#4	0.98	3.05	3.4498(17)	106.1
	C12–H12B ... S2#2	0.98	2.95	3.7522(18)	139.5
3	C1–H1A···Cl2#1	0.99	2.78	3.6987(16)	153.7

Symmetry code: **(1)** #1 $x - 1, y, z$; #2 $-x + 1/2, y + 1/2, -z + 1/2$; #3 $-x + 3/2, y + 1/2, -z + 1/2$; #4 $x - 1/2, -y + 3/2, z - 1/2$; **(1·solv)** #1 $-x + 1, -y + 1, -z + 2$; #2 $-x + 1, -y + 2, -z + 2$; #3 $x + 1, y, z$; #4 $x, y - 1, z + 1$; #5 $-x + 2, -y + 1, -z + 2$; #6 $-x, -y + 2, -z + 2$; #7 $1 - x, 1 - y, 3 - z$; **(2)** #1 $x + 1/2, -y + 3/2, z + 1/2$; #2 $-x + 3/2, y - 1/2, -z + 3/2$; #3 $x - 1/2, -y + 3/2, z + 1/2$; #4 $1 + x, y, z$; **(3)** #1 $-x + 1, y, -z + 3/2$.

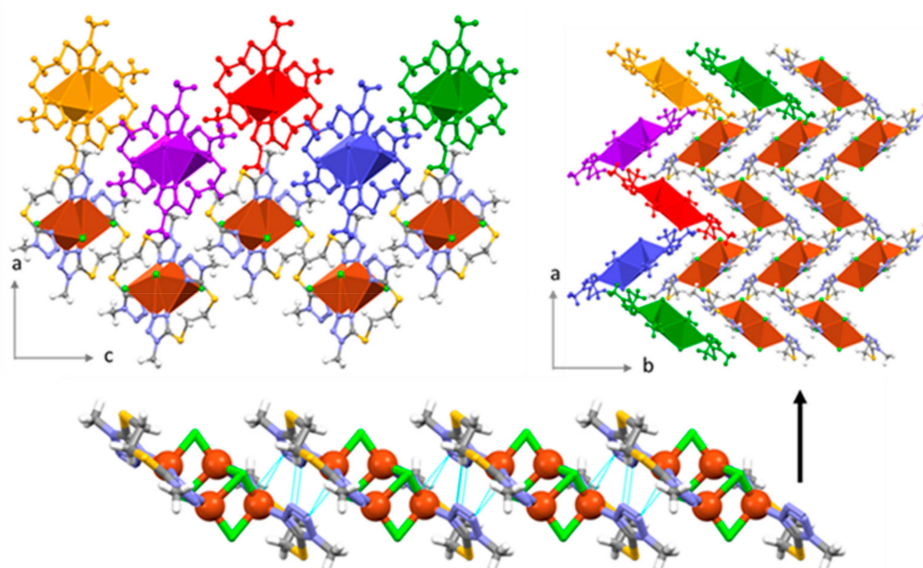


Figure 6. Supramolecular organization in the crystal structure of **2**.

2.7. Hirshfeld Surface Study

A Hirshfeld surface study was carried out to gain a fuller appreciation of the nature and quantitative contributions of intermolecular interactions to the supramolecular assembly of complexes **1**, **2** and **3**. The decomposition of contributions from different interaction types, which overlap in the full fingerprint, proved to be helpful to highlight graphically the surface regions that are involved in a specific type of intermolecular contact. The contributions to the Hirshfeld surface area from the various close intermolecular contacts are presented in the histogram in Figure 7.

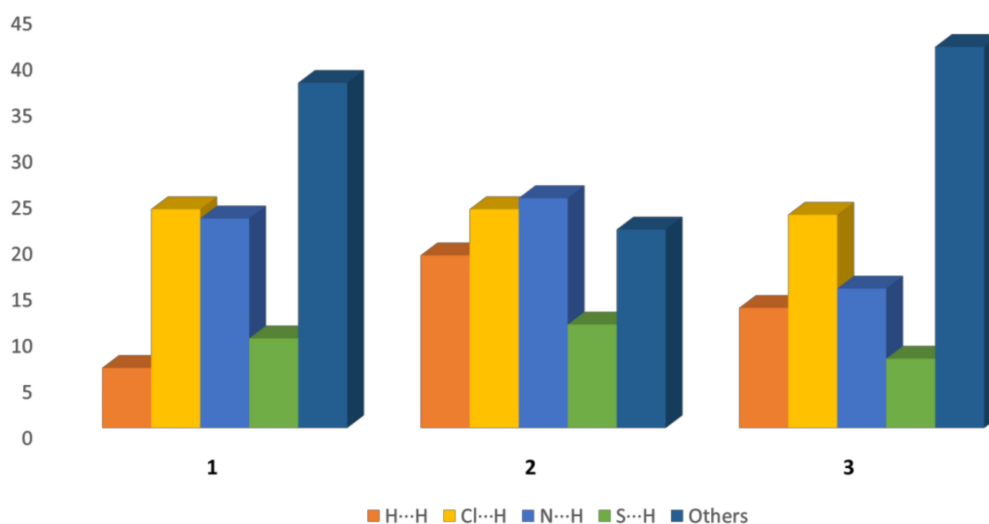


Figure 7. Contributions to the Hirshfeld surface area from the various close intermolecular contacts.

The analysis shows that in compounds **1** and **3**, the Cl...H interactions have the highest priority (the highest contribution to the Hirshfeld surface) and the N...H interactions have the highest priority in **2**.

In this approach to assess and visualize the contribution of polar and non-polar interactions to the crystal packing forces, the two-dimensional fingerprint plots for **1**, **2** and **3** were delineated for different types of contacts, such as H...H, Cl...H, N...H and S...H, as shown in Figure 8. The decomposition of contributions from different interaction types proved to be helpful to highlight graphically the surface

regions that are involved in a specific type of intermolecular contact. The visual analysis of the different fingerprint plots show that the molecular environments are clearly different in each compound.

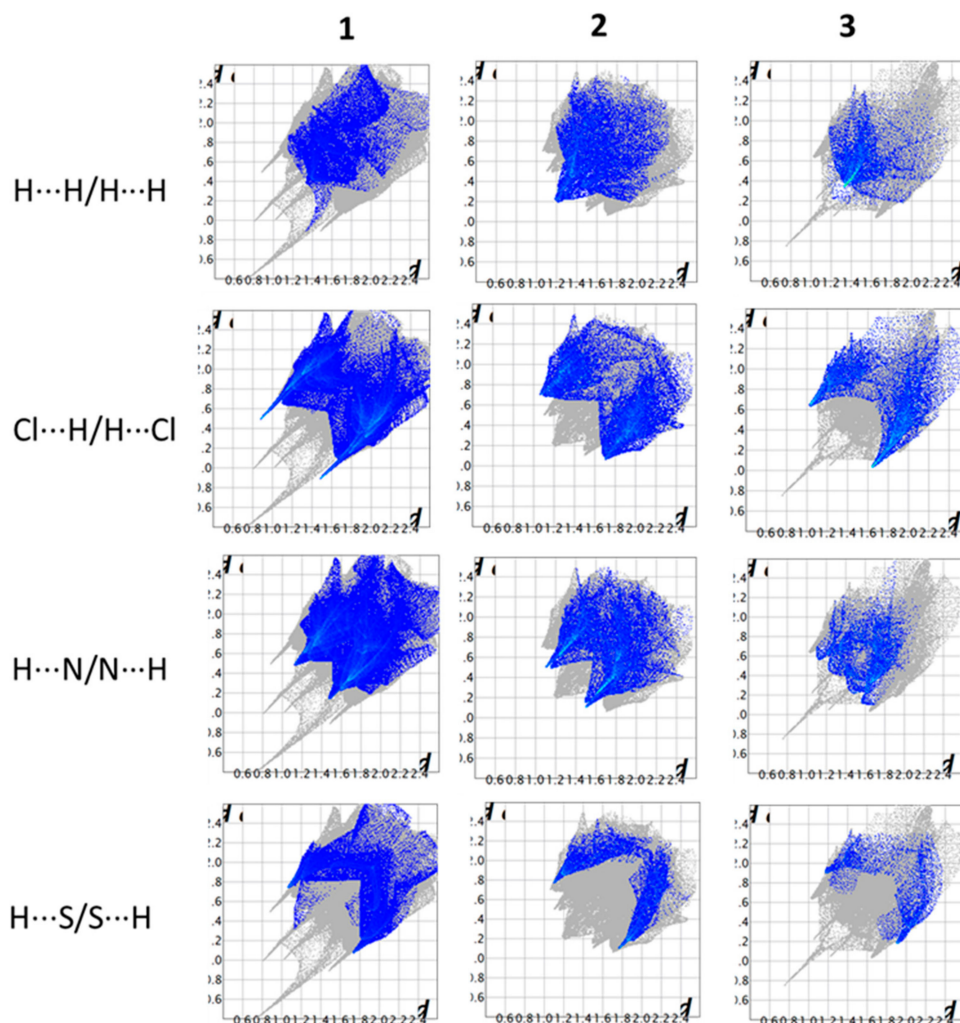


Figure 8. Fingerprint plots for H...H, Cl...H/H...Cl, H...N/N...H and H...S/S...H contacts. The outline of the full fingerprint is shown in gray.

Despite the different crystal packing arrangements, in general the Hirshfeld analysis revealed that 50%–60% of the total surface areas can be identified with Cl/H, N/H and S/H contacts, which correspond to CH...Cl, CH...N or CH...S hydrogen bonds.

The proportion of Cl...H/H...Cl interactions is almost the same in all structures and they contribute around 24% of the Hirshfeld surfaces for each compound. Furthermore, in all structures H...N contacts are present; with the highest amount in **2** (24.9%) and decreasing gradually in **1** (22.7%) and **3** (15.1%).

The H/H contacts, which are less directed than H-bonds, are present on 2D fingerprint plots as bulk central areas. These contributions correspond to the van der Waals interactions and they represent less than 20% of the Hirshfeld surfaces (barely 6.5% in **1**), thus showing that these lattices are mostly stabilized by H-bonds rather than dispersion forces. The high percentage of other interactions, as shown in Figure 7, is consistent with the number of non-classical $\pi \cdots \pi$, Cl... π or S... π interactions present in the structures. These interactions are associated with C...N, N...N, Cl...C/N and S...C/N contacts and show that tetrazole units enhance the stacking interactions in the structures. Thus, as expected, another common feature in all of the structures is the relatively low area associated with C...C interactions.

The presence of other interactions is particularly significant in the structures of **1** and **3**. The presence of water oxygen atoms in **1** produces O/H contacts that represent around 5% of the surface in this structure. Furthermore, the unsaturated coordination environment of the copper metal center in **3** gives rise to weak Cu···Cl interactions that represent around 10.2% of the total surface. These contacts are almost negligible in the other structures due to their more saturated copper coordination environments.

2.8. Thermal Analysis

The thermal stability of compounds **1**, **2** and **3** was evaluated by TGA experiments performed from room temperature to 900 °C. All of the complexes showed good thermal stability, and this indicated the strength of their corresponding networks. The least thermally stable compound was the 1D polymer **1**, which lost its coordinated water molecules (exp. 3.02%, calcd. 3.88%) at 110 °C. From 190 to 650 °C, the consecutive loss of the organic ligand and the anion occurred. Despite their different covalent dimensionality, compounds **2** and **3** were stable up to 180 °C and then began to decompose in a process that ended at 650 °C, as in compound **1**.

3. Conclusions

In the copper/chloride compounds described here, the flexible bis-tetrazole organosulfur ligands BMTTM and BMTTE have proven to be able to adopt different coordinative modes to produce different coordination geometries (tetrahedral, octahedral and square-pyramidal) around the copper ions and different covalent dimensionality (from 0D to 2D) in the resulting crystalline solids. With BMTTM, all of the synthetic methods used (except the hydro/solvothermal method) led to the same 1D coordination polymer. However, with BMTTE, the softest methods led to a 2D coordination polymer and the reaction under hydrothermal conditions led to the reduction of copper(II) to copper(I) and the crystallization of a discrete tetramer.

The supramolecular organizations in these thermally stable compounds are mainly determined by C–H···X (X = Cl, N) interactions, with a significant role of the coordinated chloride and the uncoordinated nitrogen atom of the tetrazole as acceptors and of the methyl and methylene groups of ligands as donors. Other, less common interactions, such as Cl··· π (**1**), π ··· π (**2**) and S··· π (**3**) contribute to the stabilization of the corresponding supramolecular networks, which achieve a very efficient packing. The Hirshfeld surface analysis corroborated the main geometrical observations about the crystal packing and highlight the importance of the methyl groups in establishing C–H···X (X = Cl, N or S) interactions.

4. Experimental

4.1. Materials and Physical Measurements

Solvents and reagents were obtained commercially and were used as supplied. BMTTM [30] and BMTTE [16,17] ligands were synthesized by ourselves. Elemental organic analysis (C, H, N) was carried out on a Carlo Erba 1108/Chromatographic combustion elemental analyzer. FT-IR spectra in the 4000–400 cm⁻¹ region were recorded on a Jasco FT/IR-6100 spectrophotometer. Thermogravimetric analysis (TGA) and Differential Scanning Calorimetry analysis (DSC) profiles were obtained with a TGA-ATD/DSC, SETSYS Evolution 1750 (Setaram) thermal analyzer.

4.2. Synthesis and Crystallization of the Complexes

4.2.1. $\infty^1\text{Cu}_3\text{Cl}_6(\text{H}_2\text{O})_2(\text{BMTTM})_2$ (**1**) and $\infty^1\text{Cu}_3\text{Cl}_6(\text{H}_2\text{O})_2(\text{BMTTM})_2 \cdot 4\text{CH}_3\text{CN}$ (**1·solv**)

The pseudopolymorphs **1** and **1·solv** were obtained as crystalline materials using different synthetic methodologies:

Method 1: Diffusion

To a solution of $\text{CuCl}_2 \cdot 2\text{H}_2\text{O}$ (0.25 mmol) in CH_3CN (10 mL) in a test-tube was slowly added a solution of ligand (0.25 mmol) in CH_3CN (10 mL). Blue single crystals of **1** mixed with some colorless crystals of ligand were obtained after two days. Yield: 84%.

Method 2: Microwave Irradiation

To a solution of $\text{CuCl}_2 \cdot 2\text{H}_2\text{O}$ (0.9 mmol) in CH_3CN (10 mL) was slowly added a solution of ligand (0.9 mmol) in CH_3CN (10 mL). This mixture was irradiated for 10 min in a modified conventional microwave oven [31]. After slow evaporation at room temperature, we first isolated a few prismatic blue single crystals of **1-solv** and then blue plate single crystals of **1**. Yield: 69%.

Method 3: Stirring at Room Temperature

To a solution of $\text{CuCl}_2 \cdot 2\text{H}_2\text{O}$ (0.9 mmol) in CH_3CN (10 mL) was slowly added a solution of ligand (0.9 mmol) in CH_3CN (10 mL). The mixture was stirred for 24 h at room temperature. The blue crystalline powder of **1** was filtered off and dried over CaCl_2 . Yield: 87%.

Data for **1**: MP: 170–175 °C. Anal. Calc. for $\text{C}_{10}\text{H}_{20}\text{Cl}_6\text{N}_{16}\text{O}_2\text{S}_4\text{Cu}_3$: N 24.1%, C 13.0%, H 2.2%; Found: N 24.1%, C 13.2%, H 2.4%. IR (cm^{-1}): 1480m, 1414m, 1393m, 1365m, $\nu(\text{ring})$; 1177m, $\delta(\text{CH})$; 1087m, 1039m, 1003m, $\delta(\text{ring})$; 708s, $\nu(\text{C-S})$.

4.2.2. $[\text{Cu}_2\text{Cl}_2(\text{BMTTE})]_2$ (**2**) and $\infty^2\text{Cu}_2\text{Cl}_4(\text{BMTTE})$ (**3**)

Synthesis of $[\text{Cu}_2\text{Cl}_2(\text{BMTTE})]_2$ (**2**)

A mixture of $\text{CuCl}_2 \cdot 2\text{H}_2\text{O}$ (2.7 mmol) and BMTTE (0.9 mmol) in H_2O (5–15 mL) was sealed in a 20-mL Teflon-lined autoclave and heated to 160 °C over 100 min. The autoclave was kept at 160 °C for 3 days and then slowly cooled to room temperature at a rate of 10 °C/h. Yellow single crystals of **2** were obtained.

Data for **2**: Yield: 32%. MP: 200–202 °C. Anal. calc. for $\text{C}_{12}\text{H}_{20}\text{Cl}_4\text{N}_{16}\text{S}_4\text{Cu}_4$: N 24.7%, C 15.9%, H 2.2%; Found: N 24.3%, C 15.7%, H 2.1%. IR (cm^{-1}): 1467m, 1406m, 1382m, $\nu(\text{ring})$; 1296m $\omega(\text{CH}, \text{CH}_2)$; 1173m $\delta(\text{CH})$; 1147w, 1097w, 1078w, $\delta(\text{ring})$; 728m, $\gamma(\text{CH})$; 704vs $\nu(\text{C-S})$.

Synthesis of $\infty^2\text{Cu}_2\text{Cl}_4(\text{BMTTE})$ (**3**)

Method 1: Microwave Radiation.

To a suspension of $\text{CuCl}_2 \cdot 2\text{H}_2\text{O}$ (3.56 mmol) in CH_3CN (10 mL) was slowly added a solution of ligand (0.89 mmol) in CH_3CN (10 mL). The mixture was irradiated for 10 min in a modified conventional microwave oven. After cooling (30 min), orange single crystals of **3** were obtained. Yield: 35%.

Method 2: Stirring at Room Temperature.

To a solution of $\text{CuCl}_2 \cdot 2\text{H}_2\text{O}$ (0.9 mmol) in CH_3CN (10 mL) was slowly added a solution of ligand (0.9 mmol) in CH_3CN (10 mL). After stirring at room temperature for 24 h, an orange crystalline powder was filtered off under vacuum and dried. Yield: 47%.

Data for **3**: Yield: 35%. MP: 225–230 °C. Anal. calc. for $\text{C}_6\text{H}_{10}\text{Cl}_4\text{N}_8\text{S}_2\text{Cu}_2$: N 20.40%, C 13.75%, H 1.92%; Found: N 20.80%, C 13.70%, H 1.91%. IR (cm^{-1}): 1473m, 1403m, 1384m, $\nu(\text{ring})$; 1240m $\omega(\text{CH}, \text{CH}_2)$; 1183m $\delta(\text{CH})$; 1137w, 1090w, 1052w, $\delta(\text{ring})$; 739m, $\gamma(\text{CH})$; 708vs $\nu(\text{C-S})$.

4.3. X-ray Structure Determination

Crystallographic data were collected at 293 K on a Bruker Smart 1000 CCD diffractometer using graphite-monochromated Mo- $\text{K}\alpha$ radiation ($\lambda = 0.71073 \text{ \AA}$). The software SMART [32] was used to collect frames of data, index reflections, and determine lattice parameters. SAINT [33] was used for integration of intensity of reflections and SADABS [34] for scaling and empirical absorption

correction. The structure was solved by a dual-space algorithm using the program SHELXT [35]. All non-hydrogen atoms were refined with anisotropic thermal parameters by full-matrix least-squares calculations on F^2 using the program SHELXL [35] with OLEX2 [36]. Hydrogen atoms were inserted at calculated positions and constrained with isotropic thermal parameters. Drawings were produced with Mercury [28]. Special computations for the crystal structure discussions were carried out with PLATON [37]. Crystal data and structure refinement parameters are reported in Table S1.

X-ray powder diffraction (XRPD) was performed using a Siemens D-5000 diffractometer with Cu-K α radiation ($\lambda = 1.5418 \text{ \AA}$) over the range $5.0\text{--}60.0^\circ$ in steps of 0.20° (2θ) with a count time per step of 5.0 s. The program FULLPROF [38] was used to perform profile matching between powder diffraction data and that calculated from the single-crystal structures.

4.4. Hirshfeld Surface Study

Hirshfeld surfaces and their respective 2D fingerprint plots for all complexes were calculated with CRYSTALEXPLORER 3.1 software [39]. The d_{norm} surface and the breakdown of two-dimensional fingerprint plots were used to analyze intermolecular interactions in the different crystal lattices. The sizes and shapes of the fingerprints illustrate the significant differences between the intermolecular interaction patterns.

Supplementary Materials: The following are available online at <http://www.mdpi.com/2624-8549/2/1/5/s1>, Figure S1: Infrared Spectra, Figure S2: Thermogravimetric analysis, Figure S3: Powder X-Ray Diffraction patterns, Table S1: Crystal data and structure refinement. CCDC 1971817-1971820 contains the supplementary crystallographic data for **1**, **1.solv**, **2** and **3**.

Author Contributions: Conceptualization, R.C. and A.B.L.; methodology, R.C. and O.G.-P.; synthesis, characterization, thermal analysis, O.G.-P.; formal analysis, R.C. and O.G.-P.; investigation, O.G.-P.; resources, R.C. and O.G.-P.; writing—original draft preparation, R.C. and A.B.L.; writing—review and editing, R.C., A.B.L. and E.M.V.-L.; visualization, R.C. and A.B.L.; supervision, E.M.V.-L.; project administration, R.C. and E.M.V.-L.; funding acquisition, R.C. and E.M.V.-L. All authors have read and agreed to the published version of the manuscript.

Funding: This research was funded by ERDF (EU), MEC (Spain) and Xunta de Galicia (Spain) (research projects CTQ2015-71211-REDT, CTQ2015-7091-R and ED431D 2017/01).

Acknowledgments: SC-XDR measurements were performed at the Unidade de Difracción de Raios X de Monocristal (CACTI-Universidade de Vigo), Spain. O.G.P. thanks the Xunta de Galicia for a predoctoral contract.

Conflicts of Interest: The authors declare no conflict of interest. The funders had no role in the design of the study; in the collection, analyses, or interpretation of data; in the writing of the manuscript, or in the decision to publish the results.

References

1. Hirao, T.; Kim, D.S.; Chi, X.; Lynch, V.M.; Ohara, K.; Park, J.S.; Yamaguchi, K.; Sessler, J.L. Control over multiple molecular states with directional changes driven by molecular recognition. *Nat. Commun.* **2018**, *9*, 823. [[CrossRef](#)]
2. Thomas-Gipson, J.; Pérez-Aguirre, R.; Beobide, G.; Castillo, O.; Luque, A.; Pérez-Yañez, S.; Román, P. Unravelling the Growth of Supramolecular Metal–Organic Frameworks Based on Metal–Nucleobase Entities. *Cryst. Growth Des.* **2015**, *15*, 975–983. [[CrossRef](#)]
3. Steed, J.W.; Atwood, J.L. *Supramolecular Chemistry*; John Wiley & Sons: London, UK, 2013.
4. Lehn, J.-M. *Supramolecular Chemistry*; VCH: Weinheim, Germany, 1995.
5. Taylor, R.; Kennard, O. Crystallographic Evidence for the Existence of C–H \cdots O, C–H \cdots N, and C–H \cdots Cl Hydrogen Bonds. *J. Am. Chem. Soc.* **1982**, *104*, 5063–5070. [[CrossRef](#)]
6. Desiraju, G.R.; Steiner, T. *The Weak Hydrogen Bond in Structural Chemistry and Biology*; Oxford University Press: Oxford, UK, 1999.
7. Brammer, L.; Bruton, E.A.; Sherwood, P. Understanding the Behavior of Halogens as Hydrogen Bond Acceptors. *Cryst. Growth Des.* **2001**, *1*, 277–290. [[CrossRef](#)]
8. Thallapally, P.K.; Nangia, A. A Cambridge Structural Database analysis of the C–H \cdots Cl interaction: C–H \cdots Cl $^-$ and C–H \cdots Cl–M often behave as hydrogen bonds but C–H \cdots Cl–C is generally a van der Waals interaction. *CrystEngComm* **2001**, *3*, 114–119. [[CrossRef](#)]

9. Popova, E.A.; Trifonov, R.E.; Ostrovskii, R.A. Tetrazoles for biomedicine. *Russ. Chem. Rev.* **2019**, *88*, 644–676. [[CrossRef](#)]
10. Neochoritis, C.G.; Zhao, T.; Dömling, A. Tetrazoles via Multicomponent Reactions. *Chem. Rev.* **2019**, *119*, 1970–2042. [[CrossRef](#)]
11. Wang, X.L.; Hu, H.L.; Tian, A.X. Influence of Transition Metal Coordination Nature on the Assembly of Multinuclear Subunits in Polyoxometalates-Based Compounds. *Cryst. Growth Des.* **2010**, *10*, 4786–4794. [[CrossRef](#)]
12. Wang, X.; Hu, H.; Tian, A.; Lin, H.; Li, J. Application of Tetrazole-Functionalized Thioethers with Different Spacer Lengths in the Self-Assembly of Polyoxometalate-Based Hybrid Compounds. *Inorg. Chem.* **2010**, *49*, 10299–10306. [[CrossRef](#)]
13. Wang, X.; Wang, Y.; Liu, G.; Hu, H.; Tian, A. Polyoxometalates-Directed Assembly of Inorganic-Organic Hybrid Compounds with Copper Multinuclear Nano-Cluster Based on Flexible Double Tetrazole-Based Thioether. *J. Clust. Sci.* **2011**, *22*, 211–223. [[CrossRef](#)]
14. Wang, X.; Gao, Q.; Tian, A.; Hu, H.; Liu, G. Assembly of a Series of Keggin-Based Multi- and Mono-Nuclear Structures by Tuning the Bis (Tetrazole)-Functionalized Thioether Ligands. *Inorg. Chim. Acta* **2012**, *384*, 62–68. [[CrossRef](#)]
15. Liu, G.; Zhang, S.Z. Crystal structure of poly[(μ_4 -1-methyl-1H-tetrazole-5-thiolato- κ^3 S:S:N:N') copper(I)], $C_2H_3CuN_4S$. *Kristallogr. NCS* **2016**, *231*, 791–792.
16. Li, C.-R.; Chen, T.; Xia, Z.-Q. Bis[(1-methyl-1H-tetrazol-5-yl)sulfanyl]-ethane. *Acta Crystallogr.* **2011**, *E67*, o769. [[CrossRef](#)]
17. Argibay-Otero, S.; Gómez-Paz, O.; Carballo, R. A Monoclinic Polymorph of 1,2-Bis[(1-Methyl-1H-Tetrazol-5-yl)Sulfanyl]ethane (BMTTE). *Acta Crystallogr.* **2017**, *E73*, 1523–1525. [[CrossRef](#)]
18. Chen, K.; Shearer, J.; Catalano, V.J. Subtle Modulation of $Cu_4X_4L_2$ Phosphine Cluster Cores Leads to Changes in Luminescence. *Inorg. Chem.* **2015**, *54*, 6245–6256. [[CrossRef](#)] [[PubMed](#)]
19. Robin, A.Y.; Fromm, K.M. Coordination polymer networks with O- and N-donors: What they are, why and how they are made. *Coord. Chem. Rev.* **2006**, *250*, 2127–2157. [[CrossRef](#)]
20. Xue, K.; Chai, W.X.; Wu, Y.W.; Ling, C.; Song, L. Syntheses, Structures and Properties of Two Coordination Polymers Built Upon Copper(I, II) Halide Clusters and a New Thiodiazole Ligand. *J. Clust. Sci.* **2014**, *25*, 1005–1017. [[CrossRef](#)]
21. Addison, A.W.; Rao, T.N.; Reedij, J.; van Rijn, J.; Verschoor, G.C. Synthesis, structure, and spectroscopic properties of copper(II) compounds containing nitrogen–sulphur donor ligands; the crystal and molecular structure of aqua [1,7-bis(N-methylbenzimidazol-2'yl)-2,6-dithiaheptane] copper(II) perchlorate. *J. Chem. Soc. Dalton Trans.* **1984**, *7*, 1349–1356. [[CrossRef](#)]
22. Amoedo, A.; Carballo, R.; García-Martínez, E.; Lago, A.B.; Vázquez López, E.M. Molecular metallocycles, acyclic metallodimers and 2D coordination polymers containing the twisted ligand bis(pyrimidin-2-ylthio)methane. *Dalton Trans.* **2010**, *39*, 2385–2394. [[CrossRef](#)]
23. Li, L.; Li, H.; Ren, Z.; Lang, J. Unique Deca- and Tetranuclear Halocuprate(I) Clusters of a Clamplike Ligand: Isolation, Structure, and Luminescence Properties. *Eur. J. Inorg. Chem.* **2014**, *5*, 824–830. [[CrossRef](#)]
24. Kwon, H.; Lee, E. Static and dynamic coordination behaviours of copper(I) ions in hexa(2-pyridyl)benzene ligand systems. *Dalton Trans.* **2018**, *47*, 8448–8455. [[CrossRef](#)] [[PubMed](#)]
25. Mehrotra, P.K.; Hoffmann, R. Copper(I)-copper(I) interactions. Bonding relationships in d^{10} - d^{10} systems. *Inorg. Chem.* **1978**, *17*, 2187–2189. [[CrossRef](#)]
26. Yang, L.; Powell, D.R.; Houser, R.P. Structural Variation in Copper(I) Complexes with Pyridylmethanamide Ligands: Structural Analysis with a New Four-Coordinate Geometry Index, $\tau(4)$. *Dalton Trans.* **2007**, 955–964. [[CrossRef](#)] [[PubMed](#)]
27. Kitaigorodskii, A.I. *Molecular Crystals and Molecules*; Academic Press: New York, NY, USA, 1973.
28. Lago, A.B.; Carballo, R.; Rodríguez-Hermida, S.; Vázquez-López, E.M. Copper(II) Acetate/Bis(4-pyridylthio)methane System: Synthesis, Structural Diversity, and Single-Crystal to Single-Crystal Transformation. *Cryst. Growth Des.* **2014**, *14*, 3096–3109. [[CrossRef](#)]
29. Macrae, C.F.; Edgington, P.R.; McCabe, P.; Pidcock, E.; Shields, G.P.; Taylor, R.; Towler, M.; van de Streek, J. Mercury: Visualization and analysis of crystal structures. *J. Appl. Cryst.* **2006**, *39*, 453–457. [[CrossRef](#)]
30. Wei, W.; Xia, Z.-Q.; Chen, A.-P.; Gao, S.-L. Bis[(1-methyl-1H-tetrazol-5-yl)sulfanyl]-methane. *Acta Crystallogr.* **2011**, *E67*, o999. [[CrossRef](#)]

31. Ardon, M.; Hayes, P.D.; Hogarth, G. Microwave-Assisted Reflux in Organometallic Chemistry: Synthesis and Structural Determination of Molybdenum Carbonyl Complexes. An Intermediate-Level Organometallic-Inorganic Experiment. *J. Chem. Educ.* **2002**, *79*, 1249–1251. [[CrossRef](#)]
32. SMART, Version 5.054; Bruker AXS: Madison, WI, USA, 1997.
33. SAINT, Version 8.38A; Bruker AXS: Madison, WI, USA, 2017.
34. Sheldrick, G.M. SADABS, Version 2016/2; Program for Absorption Corrections; Göttingen University: Göttingen, Germany, 1996.
35. Sheldrick, G.M. Crystal Structure Refinement with SHELXL. *Acta Crystallogr.* **2015**, *C71*, 3.
36. Dolomanov, O.V.; Bourhis, L.J.; Gildea, R.J.; Howard, J.A.K.; Puschmann, H. OLEX2: A complete structure solution, refinement and analysis program. *J. Appl. Cryst.* **2009**, *42*, 339–341. [[CrossRef](#)]
37. Spek, A.L. Structure validation in chemical crystallography. *Acta Crystallogr.* **2009**, *D65*, 148–155. [[CrossRef](#)]
38. Rodriguez-Carvajal, J. Fullprof: A Program for Rietveld Refinement and Pattern Matching Analysis. In Proceedings of the Satellite Meeting on Powder Diffraction of the XV Congress of the IUCr, Toulouse, France, 19–28 July 1990; p. 127.
39. Wolff, S.K.; Grimwood, D.J.; McKinnon, J.J.; Turner, M.J.; Jayatilaka, D.; Spackman, M.A. *CrystalExplorer*, Version 3.1; University of Western Australia: Crawley, Australia, 2012.



© 2020 by the authors. Licensee MDPI, Basel, Switzerland. This article is an open access article distributed under the terms and conditions of the Creative Commons Attribution (CC BY) license (<http://creativecommons.org/licenses/by/4.0/>).